Transactions of the Materials Research Society of Japan 32[3] 661-664 (2007)

Structural and electrochemical properties of $Li[Ni_{1/2-x/2}Mn_{1/2-x/2}Li_x]O_2$

Yasuhiro Fujii, Hiroshi Miura, Naoto Suzuki, Masaki Okada, and Noriaki Nakayama*
Tosoh Co., Ltd, 4560 Kaisei-cho, Syunan, Yamaguchi 746-8501, Japan
Fax: 81-834-63-9896, e-mail: ya_fujii@tosoh.co.jp
*Faculty of Engineering, Yamaguchi University, 2-16-1 Tokiwadai, Ube, 755-8611, Japan
Fax: 81-836-85-9601, e-mail: nakayamn@yamaguchi-u.ac.jp

The structure and electrochemical properties of $Li[Ni_{1/2-x/2}Mn_{1/2-x/2}Li_x]O_2$ ($0 \leq x \leq 1/5$) with a layered rock-salt type structure have been investigated. The samples were prepared by the co-precipitation of Ni-Mn double hydroxides and the subsequent solid state reaction with LiOH. The electron diffraction indicates a $[\sqrt{3} \times \sqrt{3}]$ R30 ° type ordering in the transition metal layers and the order parameters increase with increasing x. Rietveld refinements of X-ray diffraction patterns for $Li[Ni_{1/2-x/2}Mn_{1/2-x/2}Li_x]O_2$ indicate some cationic disorders of Li^+ and Ni^{2+} between 3a and 3b-sites. The fraction of extra- Ni^{2+} in the Li layers is reduced with increasing the Li composition. The electrochemical properties were discussed based on the crystal structure and the morphology.
Key words: Li-ion battery, Lithium nickel manganese oxide, Electron diffraction, Cation disorder

1. Introduction

In recent years, Li-Ni-Mn-O compounds with a layered rock-salt type structure have been proposed as possible alternatives to $LiCoO_2$ widely used in current Li-ion batteries [1, 2]. These materials are superior to $LiCoO_2$ in the point of specific capacity, thermal stability, toxicity and material cost. Above all, $LiNi_{1/2}Mn_{1/2}O_2$ with α-$NaFeO_2$ type structure is one of the most possible candidates [3]. Many crystallographic studies of $LiNi_{1/2}Mn_{1/2}O_2$ have been reported for several years. Some site exchanges between Li and transition metal layers have been reported, even for the nominally stoichiometric material [4]. The cationic arrangement in the transition metal layers (3b-site) has been also investigated in several studies [5, 6]. However, the crystal structure of $LiNi_{1/2}Mn_{1/2}O_2$ is still controversial. We have synthesized $Li[Ni_{1/2-x/2}Mn_{1/2-x/2}Li_x]O_2$ to investigate the effects of excess Li atoms in the transition metal layers. The samples were characterized by using powder X-ray diffraction (XRD), electron diffraction (ED) and electrochemical measurements to clarify the correlations among the crystal structure, morphology and electrochemical properties.

2. Experimental

$Li[Ni_{1/2-x}Mn_{1/2-x}Li_x]O_2$ (x = 0, 1/13, 1/7 and 1/5) was prepared by reacting the stoichiometric amount of a double hydroxide of nickel and manganese with lithium hydroxide at 900 °C for 12 hrs in air. The chemical compositions and the average oxidation states of transition metals were determined by ICP-AES and iodometric titration, respectively. The crystal structures were identified and characterized by powder XRD and ED methods. XRD patterns were refined by the Rietveld method using Rietan-2000. A field emission type TEM (JEOL JEM2010F) was used for ED measurements. The BET specific surface area of the powder was measured with a Micrometrics Flowsorb III. SEM images were observed with a Hitachi S-4500 electron microscope. The electrochemical characteristics of cathodes were examined in CR2032 type coin cells. The cell was comprised of a cathode and lithium metal anode separated by a polypropylene separator and glass fiber mat. The cathode consisted of 25 mg of $Li[Ni_{1/2-x/2}Mn_{1/2-x/2}Li_x]O_2$ and 12 mg conducting binder pressed on a stainless screen. The electrolyte solution was 1 M $LiPF_6$/EC and DMC. The EC and DMC were mixed in a 1:2 volume ratio. The cell was charged and discharged in the voltage range of 2.5-4.3 V at a current density of 0.1-10 mA cm^{-2} at 23 °C.

3. Results and discussion

3.1 Chemical analysis

Table 1 shows the results of chemical analysis. The chemical compositions were normalized to be two oxygen atoms per formula unit. The actual compositions of these materials are very close to the nominal ones. The average oxidation state of transition metals increases monotonically with x, and agrees with the valence number calculated from the chemical compositions. $LiNi_{1/2}Mn_{1/2}O_2$ is known to have the valence state described as $LiNi^{2+}{}_{1/2}Mn^{4+}{}_{1/2}O_2$ from the XANES measurements [4]. Manganese ions are not easily oxidized to higher than 4+ in this synthesis condition. Therefore, the nickel ions should be oxidized from 2+ to 3+ to compensate the increase of Li composition. The valence state of the sample with x = 1/5 is well described as $Li[Ni^{3+}{}_{2/5}Mn^{4+}{}_{2/5}Li_{1/5}]O_2$ based on the above assumption. We have tried to prepare the sample with x > 1/5. However, the single phase materials could not be obtained. The sample prepared in this study can be represented as $Li[Ni^{2+}{}_{1/2-5x/2}Ni^{3+}{}_{2x}Mn^{4+}{}_{1/2-x/2}Li_x]O_2$ ($0 \leq x \leq 1/5$).

3.2 Crystal structure

3.2.1 XRD patterns

Figure 1 (a) shows the XRD patterns of $Li[Ni_{1/2-x/2}Mn_{1/2-x/2}Li_x]O_2$ with x = 0, 1/13, 1/7 and 1/5. All the intense peaks can be indexed based on α-$NaFeO_2$ type structure (space group: $R\bar{3}m$). However, extra

peaks around 2 θ = 20 ° in the enlarged patterns shown in Fig. 1 (b) cannot be indexed. The intensity of extra peaks increases as the Li content increases. The extra peak positions do not agree with those of Li_2MnO_3 impurities. The *d*-values (Å) of the two extra peaks correspond to 3 fold values of *d* (11.0) and *d* (11.3), respectively. For example, in the case of x = 1/13, *d* (1/3 1/3.0) is equal to be 4.316 Å and actually observed *d*-value is 4.323 Å. Therefore, the extra peaks at around 2 θ = 20 ° arise from some cation orderings in the transition metal layers.

Table 1. Chemical compositions of $Li[Ni_{1/2-x/2}Mn_{1/2-x/2}Li_x]O_2$.

	Sample of $Li[Ni_{1/2-x/2}Mn_{1/2-x/2}Li_x]O_2$			
	x = 0	x = 1/13	x = 1/7	x = 1/5
Ni/Mn atomic ratio	1.01 (1.00)	1.00 (1.00)	1.01 (1.00)	1.01 (1.00)
Li/(Ni+Mn) atomic ratio	1.04 (1.00)	1.18 (1.17)	1.35 (1.33)	1.56 (1.50)
Average valence of Ni and Mn	3.10 (3.06)	3.19 (3.21)	3.37 (3.38)	3.49 (3.55)

The numerals in parentheses represent nominal atomic ratios and oxidation states calculated from the measured compositions.

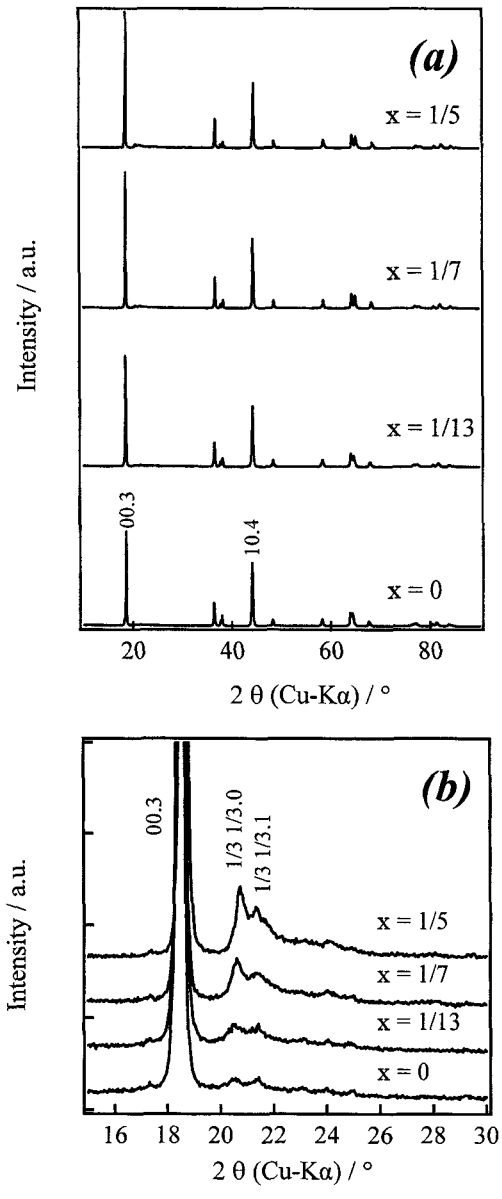

Fig. 1. (a) Powder XRD patterns of $Li[Ni_{1/2-x/2}Mn_{1/2-x/2}Li_x]O_2$ (x = 0, 1/13, 1/7 and 1/5). (b) The enlarged XRD patterns for $Li[Ni_{1/2-x/2}Mn_{1/2-x/2}Li_x]O_2$. The diffraction peaks have been indexed in hexagonal setting.

3.2.2 Rietveld refinement

Table 2 shows the structural parameters determined by Rietveld refinement for the XRD patterns of $Li[Ni_{1/2-x/2}Mn_{1/2-x/2}Li_x]O_2$. Ideally, all the 3a-sites are occupied with Li atoms, and the remaining Li atoms occupy the 3b-sites together with the transition metals. However, this model does not reproduce the observed profiles. The site exchange of Li atoms with Ni atoms should be assumed. The R_{wp} increases with increasing Li composition x. Because the present Rietveld refinements are based on the α-$NaFeO_2$ type structure ($R\bar{3}m$), the growth of extra peaks at around 2 θ = 20 ° has caused the increase of R_{wp}. As shown in Fig. 2, the Ni fraction in the Li layers decreases with the substitution of Li for transition metals. The lattice constants, as well as *c/a* ratios, vary linearly with increasing x, indicating that $Li[Ni_{1/2-x/2}Mn_{1/2-x/2}Li_x]O_2$ ($0 \leq x \leq 1/5$) solid solutions are obtained. As the Li-substitution increases, both lattice constants, *a* and *c*, tend to decrease. This may be mainly caused by the oxidation from larger Ni^{2+} to smaller Ni^{3+}. The larger *c/a* ratio indicates the less disorder of layered structure [7]. These results may support that the amount of the extra-nickel ions in the Li layers decreases in proportion to the Li composition.

Table 2. Rietveld refinements of the XRD pattern for $Li[Ni_{1/2-x/2}Mn_{1/2-x/2}Li_x]O_2$.

Structural Parameters	x = 0	x = 1/13	x = 1/7	x = 1/5
a/Å	2.8995	2.8779	2.8679	2.8569
c/Å	14.3295	14.2664	14.2429	14.2235
O(z)	0.2422	0.2418	0.2418	0.2417
g(Li1) at 3a site	0.900	0.933	0.954	0.970
g(Ni1) at 3a site	0.100	0.067	0.046	0.030
g(Li2) at 3b site	0.011	0.040	0.081	0.124
g(Ni2+Mn) at 3b site	0.988	0.960	0.919	0.876
B at 3a site	0.22	0.54	0.97	1.07
B at 3b site	0.30	0.31	0.33	0.25
B at 6c site	0.38	0.38	0.35	0.28
Rwp/%	9.72	10.45	12.96	15.90

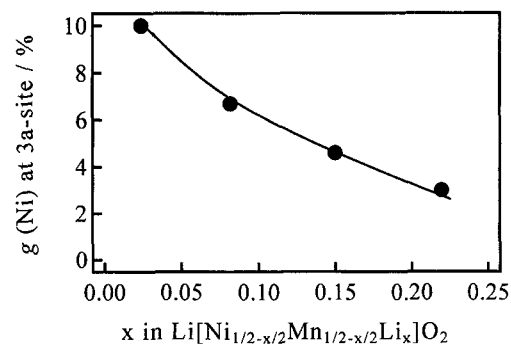

Fig. 2. Ni-occupancy at 3a-sites of $Li[Ni_{1/2-x/2}Mn_{1/2-x/2}Li_x]O_2$ refined by Rietveld method.

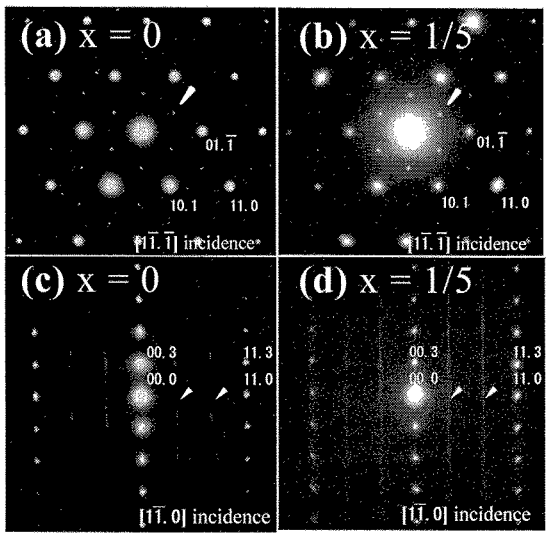

Fig. 3. ED patterns of $Li[Ni_{1/2-x/2}Mn_{1/2-x/2}Li_x]O_2$ (x = 0 and 1/5). The diffraction spots have been indexed assuming the $R\bar{3}m$ structure in hexagonal setting. The extra spots and the diffuse streaks due to the in plane $[\sqrt{3} \times \sqrt{3}]R30°$ orderings are marked by arrows.

3.2.3 ED patterns

Figures 3 (a) and (b) show the $[1\bar{1}.\bar{1}]$ zone electron diffraction patterns (EDPs) and Fig. 3 (c) and (d) show the $[1\bar{1}.0]$ zone EDPs of rhombo-hexagonal $Li[Ni_{1/2-x/2}Mn_{1/2-x/2}Li_x]O_2$ (x = 0 and 1/5), respectively. The $[1\bar{1}.\bar{1}]$ zone EDPs show the extra spots, as marked by arrows in the figures, indicating a $[\sqrt{3} \times \sqrt{3}]R30°$ type ordering in the basal plane [8]. Because of the multiple twining, all the EDPs are rather complex. $[1\bar{1}.0]$ zone EDPs also show the diffuse streaks along the c^* axis indicating the stacking disorder of the ordered layers. It should be noted that the extra spots and the diffuse streaks in the EDPs of $Li[Ni_{1/2-x/2}Mn_{1/2-x/2}Li_x]O_2$ become more intense with increasing x.

S.H. Choi et al. has reported these extra spots might arise from the cubic spinel phase and also reported that the XRD pattern of $Li_{1+x}Ni_{0.5}Mn_{0.5}O_{2+\delta}$ (x = 0.5) indicates the co-existence of the Li_2MnO_3 impurity and a cubic spinel phase [9]. On the contrary, we indicate that the extra peaks around $2\theta = 20°$ in the XRD patterns of $Li[Ni_{1/2-x/2}Mn_{1/2-x/2}Li_x]O_2$ do not result from impurities of Li_2MnO_3, but arise from the cation ordering in the transition metals layers, because the *d*-values of the extra peaks are exactly equal to the 3-fold values of *d* (11.0) and *d* (11.3).

3.3 Morphology

Figure 4 shows BET specific surface areas and SEM images of $Li[Ni_{1/2-x/2}Mn_{1/2-x/2}Li_x]O_2$ (x = 0, 1/13, 1/7 and 1/5). As the Li content increases, the BET specific surface area tends to decrease. The samples with x = 0 and 1/13 exhibit the hexagonal habit and they show little difference in morphology and surface area. As the Li content increased further, the primary particle agglomerated dramatically and do not show the obvious hexagonal habit. In spite of disappearing the plate-like particles with hexagonal habit, the intensity ratio of the 00.3 peak to the 10.4 one becomes higher in the XRD

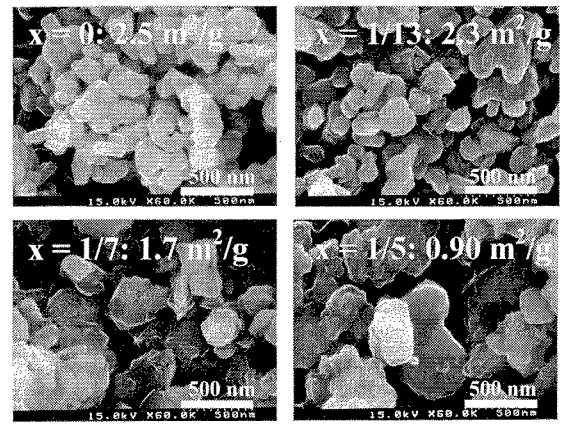

Fig. 4. SEM images and BET specific surface areas of $Li[Ni_{1/2-x/2}Mn_{1/2-x/2}Li_x]O_2$.

patterns with x = 1/7 and 1/5 as shown in Fig. 1 (a). These results support that Rietveld refinements cannot be affected by a preference orientation of hexagonal habit particles, but mainly by the decrease of the Ni-fraction at 3a-sites with increasing the Li-substitution.

3.4 Electrochemical properties

Figure 5 shows the voltage *v.s.* capacity curves for $Li/Li[Ni_{1/2-x/2}Mn_{1/2-x/2}Li_x]O_2$ cells cycled between 2.5 and 4.3 V at a rate of 0.4 mA cm^{-2}. All the samples show smooth charge and discharge curves. This indicates that $Li[Ni_{1/2-x/2}Mn_{1/2-x/2}Li_x]O_2$ remains a single phase during the charge-discharge process. The capacity tends to decrease up to x = 1/5, as the theoretical capacity based on the chemical compositions decreases with increasing x. The operating voltage of $Li[Ni_{1/2-x/2}Mn_{1/2-x/2}Li_x]O_2$ does not depend on the Li-composition, x. The redox potentials of $Li[Ni_{1/2-x/2}Mn_{1/2-x/2}Li_x]O_2$ are almost constant, although $Li[Ni_{1/2-x/2}Mn_{1/2-x/2}Li_x]O_2$ contains two types of nickel ions (Ni^{2+}/Ni^{3+}) with the different ratios corresponding to the chemical compositions. The redox potentials of $LiNi_{1-x}Mn_xO_2$ are also constant and irrelevant to Ni^{2+}/Ni^{3+} ratio [4].

Figure 6 shows the dependence of the discharge capacity on the current densities for $Li/Li[Ni_{1/2-x/2}Mn_{1/2-x/2}Li_x]O_2$ cells. Discharge currents were varied from 0.1 to 10 mA cm^{-2}. The sample with x = 1/13 is improved compared with the sample with x = 0. Even at the higher densities of 2.5, 5.0 and 10 mA cm^{-2}, the sample with x = 1/13 delivered the highest capacity among all the samples. On the other hand, for the samples from x = 1/13 to x = 1/5, the capacity decreases as a function of x. The capacity fading should be arise from the decrease of the theoretical capacity with increasing the Li composition. The presence of Ni atoms in the Li layers can impede the diffusion of Li^+ in the solid matrix. The best performance of the sample with x = 1/13 might result from the lower structural disorders.

C.C. Chang et al. have investigated the influence of both crystal size and the cationic disorders on the electrochemical properties of $LiNiO_2$ [10]. They concluded that the electrochemical properties of $LiNiO_2$ are more strongly influenced by the cation disorders than the crystal size.

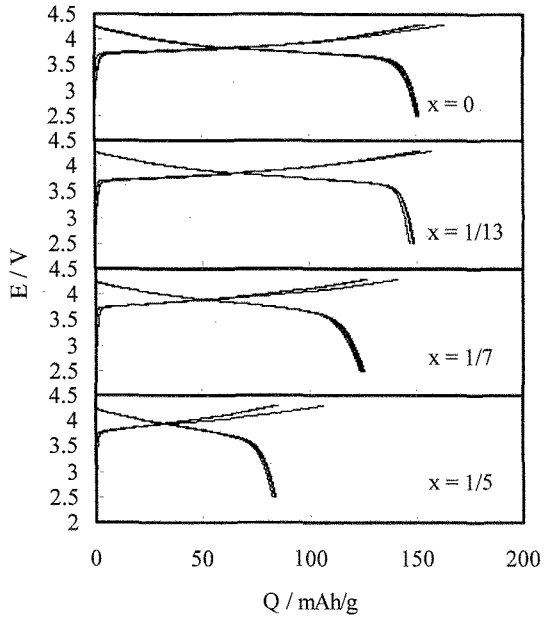

Fig. 5. Charge and discharge curves for $Li[Ni_{1/2-x/2}Mn_{1/2-x/2}Li_x]O_2$ at a rate of 0.4 $mAcm^{-2}$ in voltages of 2.5-4.3 V for 5 cycles.

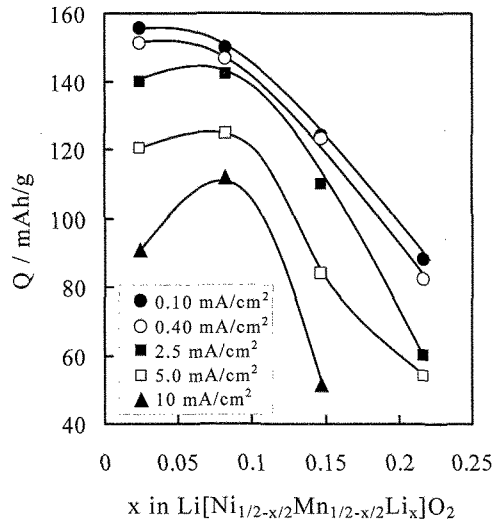

Fig. 6. Rate capabilities at different rates in voltages of 2.5-4.3 V for $Li[Ni_{1/2-x/2}Mn_{1/2-x/2}Li_x]O_2$.

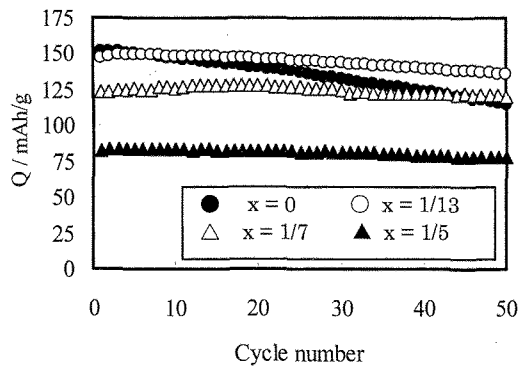

Fig. 7. Cycling stabilities at a rate of 0.4 $mAcm^{-2}$ in voltages of 2.5-4.3 V for $Li[Ni_{1/2-x/2}Mn_{1/2-x/2}Li_x]O_2$.

On the other hand, the electrochemical properties of $Li[Ni_{1/2-x/2}Mn_{1/2-x/2}Li_x]O_2$ seems to be affected not only by cation disorders but also by a primary particle size. However, the quantitative effect of above two factors on the electrochemical properties is not fully understood at the present stage. Figure 7 shows the cycle performance for $Li/Li[Ni_{1/2-x/2}Mn_{1/2-x/2}Li_x]O_2$ cells cycled between 2.5 and 4.3 V at a rate of 0.4 mA cm^{-2}. A slight deterioration was observed for the sample with x = 0, while the performances of the samples with x = 1/13, 1/7 and 1/5 are more stable than that of the sample with x = 0. The capacity retentions during cycles are higher with Li-substituted samples.

4. Conclusions

The crystal structure and the electrochemical properties of $Li[Ni_{1/2-x/2}Mn_{1/2-x/2}Li_x]O_2$ ($0 \leq x \leq 1/5$) with a layered rock-salt type structure have been investigated. The XRD and ED measurements indicate the $\sqrt{3}\times\sqrt{3}$ superlattice in the transition metal layers. The intensity of extra spots due to the superlattice increases with increasing the Li-composition. Rietveld refinements of XRD patterns also indicate the fraction of extra-nickel ion in the Li layers decreases and the fraction of Li ion in the transition metals layers increases as a function of x. There is a strong possibility that the cationic ordering in the basal plane might originate from the ordering of Li^+ and Mn^{4+}. The electrochemical properties are rather improved for the sample with x = 1/13 compared with the one with x = 0. The improvement can be related to the decrease of the fraction of Ni ions in the Li layers.

References

[1] E. Rossen, C.D.W. Jones, and J.R. Dahn, *Solid State Ionics*, **57**, 311-318 (1992)
[2] Z. Lu, L. Y. Beaulieu, R. A. Donaberger, C. L. Thomas, and J.R. Dahn, *J. Electrochem. Soc.*,**149** (6) A778-A791(2002)
[3] T.Ohzuku and Y.Makimura, *Chem. Lett.*, 744-745 (2001)
[4] H.Kobayashi, Y.Arachi, H.Kageyama, H.Sakaebe, K.Tatsumi, S.Emura, M.Yoneyama, D.Mori, R.Kanno, T.Kamiyama, *J. Mater. Chem.*, **13**, 590-595 (2003)
[5] Y. Koyama, Y. Makimura, I. Tanaka, H. Adachi and T. Ohzuku, *J. Electrochem. Soc.*, **151** (9) A1499 - A1506 (2004)
[6] A. Van der Ven and G. Ceder, *Electrochemistry Communications*, **6**, 1045-1050 (2004)
[7] J.M. Kim, H.T. Chung, *Electrochim. Acta* **49**, 937-944 (2004)
[8] N. Nakayama, T. Mizota, T. Ohzuku, and Y. Ueda, *Trans. Mater. Res. Soc. Jpn*, **29**, 2559-2562 (2004)
[9] S.H. Choi, O. A. Shylyakhtin, J. Kim, Y.S. Yoon, *J. Power Sources*, **140**, 355-360 (2005)
[10] C.C. Chang, J.Y. Kim, and P. N. Kumta, *J. Electrochem. Soc.*, **149** (9) A1114-A1120 (2002)

(Received January 20, 2007;Accepted May 10, 2007)